THE ASTROPHYSICAL JOURNAL, 232:485–495, 1979 September 1

VELOCITY FIELDS IN THE SHELL OF α ORIONIS

ANN MERCHANT BOESGAARD
Institute for Astronomy, University of Hawaii
Received 1978 October 30; accepted 1979 March 19

ABSTRACT

Eight new spectrograms at 6.7 Å mm^{-1} of the Fe II emission lines (3150–3300 Å) in α Ori supplement earlier material to cover a five year period with a concentration of six spectra over a 64 day interval. The emission-line radial velocities follow the same pattern of variations as the photospheric lines but are redshifted by $+5$ km s^{-1}. The emission at Ca II H and K is also redshifted: $+6$ km s^{-1}. The shell is modeled as a spherical moving envelope following Kunasz and Hummer, and calculated line profiles are compared with observed. The effects of the various model parameters (size, density distribution, velocities, optical depth, etc.) on the calculated profiles are discussed. The great widths of the observed emission lines must be due to high fluid and turbulent velocities. The parameters which result in the best match for the strong, self-reversed Fe II line at 3228 Å also produce good fits for two weak lines and two intermediate-strength lines as well. In this model the shell is about 1.8 stellar radii, and material is accelerating inward from about 15 km s^{-1} at 1.8 R_* to 60 km s^{-1} at R_*. The free-fall velocity is 61 km s^{-1}, and the sonic velocity is 9 km s^{-1}. Turbulence will be generated in the shell, and the values required for the profile fit are 9 km s^{-1} for microturbulence and 8 km s^{-1} for macroturbulence, i.e., marginally subsonic turbulence. The material and velocities in this inner shell region may arise from the motions of the large convective cells hypothesized by Schwarzschild in the photospheres of red giants or supergiants. The mechanical energy provided by the motions in the stellar atmosphere and the supersonic infall can provide the thermal and turbulent energy in the interface between the photosphere and the circumstellar shell. A picture of the complex, extensive shell is presented.

Subject headings: stars: chromospheres — stars: circumstellar shells — stars: individual — stars: late-type — stars: supergiants

I. INTRODUCTION

There have been several recent observational studies of mass loss in late-type stars and the physical conditions in the circumstellar (CS) shells[1] (Reimers 1975; Sanner 1976; Bernat 1977; Hagen 1978; Boesgaard and Hagen 1979). However, the mechanism for the mass loss in these stars is uncertain as discussed in the review by Weymann (1977). Schwarzschild (1975) and Goldberg (1976) suggest that the origin of the CS shells is probably connected with convection in the lower layers. Schwarzschild (1975) examines which physical characteristics in the Sun may be responsible for the size of the convective cells there and applies this logic to models of red giant envelopes and then estimates that the size of the convective cells in cool giants and supergiants is such that only a few exist at one time on the stellar surface. Schwarzschild considers what he calls an extreme hypothesis: that the dominant convective cells control the integrated brightness variations since so few exist at one time, and the temperature differential between hot, rising and cool, falling material is on the order of 1000 K. He finds characteristic time scales for the irregular variations from the estimated dimensions ($\sim 8 \times 10^7$ km) and velocities (~ 5 km s^{-1}) of the cells to be about 150–200 days compared with observed variations of 100–300 days.

In this paper we examine the evidence relevant to Schwarzschild's hypothesis and to the mass-loss mechanism provided by the velocities and line profiles of the Fe II emission lines in α Ori. These ultraviolet lines from multiplets 1, 6, and 7, first noted by Herzberg (1948), are formed in the lower layers of the CS shell or in the interface between the star and the CS shell. According to a survey by Boesgaard and Boesgaard (1976), the lines appear in the spectra of virtually all stars cooler than spectral type M1; they appear when the stellar effective temperature is low enough that there is little continuous radiation at 3100–3300 Å. In addition they found that the line strength at a given temperature is correlated with the strength of CS shell indicators and that α Ori shows the strongest Fe II emission of the stars surveyed. Weymann (1962) and Boesgaard and Magnan (1975) have observed these features at high dispersion and discussed their interpretation. A new series of six spectrograms has been obtained over a period of 64 days to cover part of the Schwarzschild cycle and to gain additional information on the velocity fields.

[1] The term CS shell, or simply shell, is used throughout for the envelope of gas and dust surrounding the star. The transition from the classical chromosphere to the CS shell is not sharp; the interface region includes the upper chromosphere and inner parts of the CS shell.

II. OBSERVATIONS AND VELOCITIES

Spectrograms at 6.7 Å mm^{-1} were obtained of α Ori which covered both the Fe II region (3150–3300 Å) and Ca II H and K (3933, 3968 Å) with the coudé spectrograph of the 2.2 m telescope at Mauna Kea. A 600 line mm^{-1} grating blazed in the second-order blue at 4000 Å was used; the resolution is $\sim$0.13 Å. The Corning 9863 filter used to block the first-order red spectrum also reduces the light at 3900 Å so that the exposure for Fe II is also good for Ca II. Spectrograms taken in 1974 and 1975 in combination with those presented by Boesgaard and Magnan (1975) cover a five year period with a concentration of six plates over a 64 day interval. Many semiregular M-type variables, such as μ Cep and X Her, show some evidence for a complex pattern of variation with both a long period (the order of several hundred days) and a short period, typically $\sim$100 days (see Payne-Gaposchkin and Gaposchkin 1938). For α Ori the long period is 2070 days but the shorter period is uncertain; the spectra were taken over the 64 day period in an attempt to cover part of the shorter period which may be a result of the Schwarzschild convective cell cycle. An example of the spectrum of α Ori in the Fe II region is shown in Figure 1 of the Boesgaard and Magnan (1975) paper.

Intensity tracings were made of the eight new spectrograms through means of the calibration stripes exposed at the time of the stellar exposure and by use of a Boller and Chivens microphotometer. Superposition of the tracings of the six spectra obtained in the 64 day interval showed no variations in the Fe II emission-strengths. The Ca II line profiles did show small changes due to the position of the deep central absorption minimum; none of the changes was as obvious as that shown by Boesgaard (1973) in the K line of α Ori.

Radial velocities were measured in the stellar photosphere for the emission and self-reversal features of Fe II and for the various emission and absorption components of the H and K lines of Ca II. Photospheric velocities were found from about 32 unblended lines with no CS components in the Fe II and Ca II regions. Both Weymann (1962) and Boesgaard and Magnan (1975) point out that some of the Fe II lines are mutilated by absorption features; Table 1 lists the unblended lines. For this study the velocities of only five to six strong self-reversed Fe II lines have been measured on each spectrogram. For both Fe II and Ca II lines the position of the emission feature was measured by the midpoint of the total emission at approximately half-intensity on a Grant measuring machine. The broad photospheric Ca II absorption (as well as the presence of the deep central absorption reversal) makes this measurement less reliable for the Ca II lines than for the Fe II lines, which show steep-sided emission with a central reversal. The position of the deepest part of the self-reversal was measured for both Fe II and Ca II also.

Table 2 gives the measured velocities and probable errors for the photosphere, the Fe II and Ca II emission, and the Fe II and Ca II reversals for each spectrogram. The results for the Ca II lines are the mean of both the H and K lines since the influence of the Hϵ line on the H line in this star is indiscernible. The data given by Boesgaard and Magnan (1975) (Table 2 and Figure 4) show that variations in the velocities of the Fe II emission lines follow the same pattern as those of the photospheric absorption lines. This is further demonstrated in Figure 1 which shows the linear correlation of photospheric velocity with emission-line velocities for both Ca II and Fe II (for the new and the old spectrograms). This implies that the layers in which the emission is formed moves with the photosphere. Furthermore, on *all* eight of the new spectra the emission of *both* Ca II and Fe II is redshifted relative to the photospheric lines. The mean redshift of the Ca II emission is $+5.9 \pm 1.3$ km s^{-1} and of the Fe II emission, including the Boesgaard and Magnan data, is $+5.1 \pm 1.0$ km s^{-1}. (Errors quoted are probable errors of the mean.) Wilson and Bappu (1957) give a redshift of 4 km s^{-1} for the Ca II K2 emission in α Ori.

The positions of the reversals for the two ions differ, however. The reversals for the Fe II lines are red-shifted relative to the photosphere with a mean value of $+7.2 \pm 0.9$ km s^{-1}, whereas the central absorption in the H and K lines is always blueshifted with a mean of -4.7 ± 1.4 km s^{-1}. Thus the major portion of the

TABLE 1

UNBLENDED Fe II EMISSION LINES

Lab λ (Å)	Multiplet	Ex. Pot. (low–high) (eV)	Transition	Reversal?
3163.091..........	7	1.66–5.57	$^4P_{5/2}$–$^4F^{\circ}_{5/2}$	No
3166.670..........	6	1.69–5.56	$^4P_{5/2}$–$^4D^{\circ}_{3/2}$	No
3170.337..........	6	1.69–5.58	$^4P_{3/2}$–$^4D^{\circ}_{1/2}$	No
3185.315..........	7	1.72–5.59	$^4P_{1/2}$–$^4F^{\circ}_{3/2}$	No
3186.740..........	6	1.69–5.56	$^4P_{3/2}$–$^4D^{\circ}_{3/2}$	Yes
3193.809..........	6	1.72–5.58	$^4P_{1/2}$–$^4D^{\circ}_{7/2}$	Yes
3196.070..........	7	1.66–5.52	$^4P_{5/2}$–$^4F^{\circ}_{7/2}$	Yes
3210.449..........	6	1.72–5.56	$^4P_{1/2}$–$^4D^{\circ}_{3/2}$	Yes
3227.732..........	6	1.66–5.49	$^4P_{5/2}$–$^4D^{\circ}_{7/2}$	Yes
3277.347..........	1	0.98–4.75	$^4D_{7/2}$–$^6D^{\circ}_{9/2}$	Yes

TABLE 2

MEASURED VELOCITIES FOR THE PHOTOSPHERE, Fe II AND Ca II EMISSION AND Fe II AND Ca II SELF-REVERSED ABSORPTION

Plate Number	KE-1714	KE-1720	KE-1816	KE-1827	KE-1888	KE-1901	KE-2179	KE-2271	Mean
Julian Day 2442+	316.13	317.15	344.14	346.09	378.06	379.99	661.13	728.62	
Photosphere (Fe region) km/s	22.4 ±0.5	22.9 ±0.4	23.5 ±0.3	23.0 ±0.4	22.6 ±0.3	23.1 ±0.4	20.5 ±0.4	21.9 ±0.6	
Fe II Emission	25.6 ±0.8	25.7 ±0.8	28.4 ±0.7	26.5 ±1.2	28.0 ±0.7	29.6 ±0.6	27.1 ±0.9	26.4 ±0.9	
Emis-Photosphere	+3.2	+2.8	+4.9	+3.5	+5.4	+6.5	+6.6	+4.5	4.7±1.0
Fe II Reversals	31.2 ±1.0	28.0 ±0.6	32.3 ±0.6	30.7 ±0.5	30.2 ±0.4	29.6 ±0.7	26.4 ±0.9	29.3 ±0.7	
Fe II Rev-Photosphere	+8.8	+5.1	+8.8	+7.7	+7.6	+6.5	+5.9	+7.4	7.2±0.9
Photosphere (Ca II region)	26.0 ±0.4	24.5 ±0.3	25.4 ±0.3	25.1 ±0.3	24.5 ±0.3	23.9 ±0.3	19.5 ±0.3	21.8 ±0.3	
Ca II Emission	33.4 ±2.9	31.4 ±0.2	32.8 ±0.4	28.2 ±2.0	28.2 ±2.2	29.6 ±3.7	24.2 ±0.9	30.4 ±0.8	
Ca II Emis-Photosphere	+7.4	+6.9	+7.4	+3.1	+3.7	+5.7	+4.7	+8.5	5.9±1.3
Ca II Reversals	18.9 ±0.7	18.7 ±0.1	19.3 ±0.3	18.9 ±0.1	20.9 ±0.3	18.2 ±0.1	17.4 ±0.1	20.5 ±0.1	
Ca II Rev-Photosphere	-7.1	-5.8	-6.1	-6.2	-3.6	-5.7	-2.1	-1.3	-4.7±1.4

absorption at H and K (which shows zero residual flux) is assumed to be formed in the expanding circumstellar shell, i.e., we are observing primarily circumstellar components (H4 and K4) rather than the chromospheric H3 and K3 reversals. The reversals observed in the Fe II lines are more probably chromospheric in origin, i.e., formed in the same region as the Fe II emission. The excitation potentials of the lower level of the Fe II lines are 1.0–1.7 eV compared with the blueshifted, "zero-volt" lines ($\lesssim 1$ eV) formed in the extended shell.

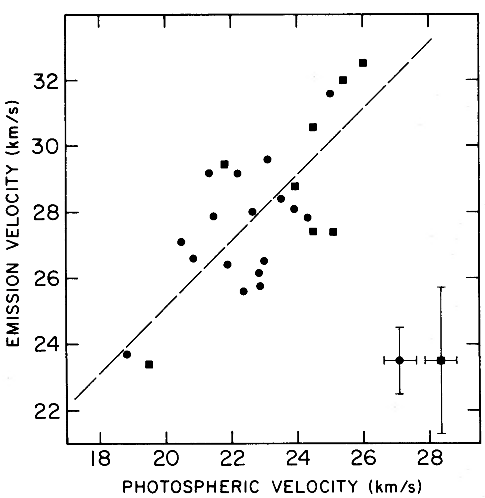

FIG. 1.—The emission-line velocity versus the photospheric velocity for α Ori. The filled circles represent the Fe II emission and the filled squares the Ca II emission reduced by 0.8 km s^{-1} to be on the same scale as the Fe II velocity. Typical error bars are shown for both types of points in the lower right corner. The dashed line is at a 45° slope with a displacement corresponding to the mean redshift of the emission lines, 5.1 km s^{-1}.

The evidence from the velocity measures is that the Ca emission, the Fe emission, and Fe self-reversals are formed in a region between the photosphere and the extended CS shell; within this region the motion of the line-forming matter is primarily infall, as indicated by the redshifts, superposed on an overall motion shared with the photosphere. This interface region is influenced by the motions which cause the variations in the radial velocities of the photospheric lines. The only measurable *intensity* variations on this series of spectrograms was apparently due to the small relative velocity shifts between K3 and K4, and H3 and H4. (The K4 and H4 components presumably are formed further out in the [CS] shell.) No variations in the intensities or the velocities *relative to the photosphere* were found in the inner shell region in the time series covered by the six spectra taken in the fall of 1974 nor in two taken a year later. Therefore a composite of the intensity tracings could be made of the six spectrograms for 1974; the line-profile calculations discussed in § IV were compared with the observed composite profiles. The composite line profile for the strongest Fe II line, λ3228, is shown in Figure 2.

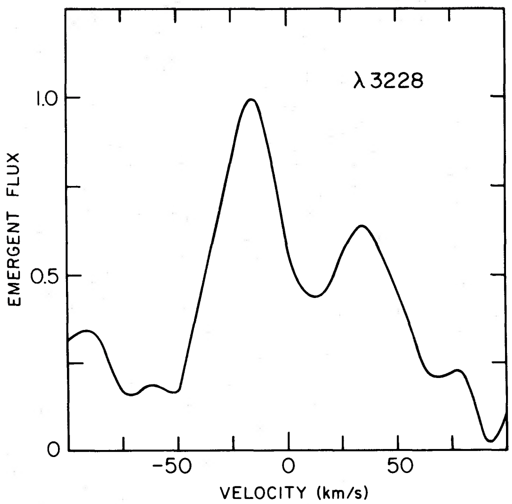

FIG. 2.—The observed emission line profile for Fe II λ3228 in α Ori. The maximum flux is normalized at 1.0 which puts the local continuum at 0.3. Note the breadth of the emission feature and its redward displacement from 0 km s^{-1} as defined by the photospheric absorption lines.

Thus, the circumstantial evidence from the observed velocities and intensities gives a picture of an extended inner shell region with long-term variations similar to those of the photosphere, but with the observable matter in the shell falling back onto the star. Even though there is no convincing cycle of the order of 100 days, the fact that the emission-line velocities follow the same pattern of variations as the photospheric-line velocities tends to support Schwarzschild's suggestion that the envelope is maintained by the photospheric convection. More detailed theoretical analyses of the line profiles are presented in the next two sections.

III. THEORETICAL MODEL

Boesgaard and Magnan (1975) found that a model with an extended envelope and a fluid velocity approximately equal to the Doppler velocity was appropriate for the Fe II emission lines in α Ori. Therefore we have adapted the method developed by Hummer, Kunasz, and Kunasz (1973) for a spherical, moving envelope in which the radial velocity is not more than a few times the Doppler velocity. Some relevant details can also be found in the works of Kunasz and Hummer (1974) and Kunasz (1974). Their model is based on a two-level atom and complete redistribution in the fluid frame. The radiative-transfer equation is solved at points along a ray parallel to the line of sight; many such points and frequencies are needed in a large spherical envelope. The original codes have been modified, however, for this study. We do not try to solve specifically for the line-source function, but rather parametrize it, as did Boesgaard and Magnan (1975), in the form

$$S(\tau) = S_0(\tau/S_1T)^{1/2}e^{-\tau/S_1T}$$

to mimic a chromospheric temperature rise and then a subsequent decline due to radiation losses. In the above equation τ is the line optical depth at the mean wavelength integrated along the radius, T is the total radial optical depth, and S_1T represents the optical depth where the source function reaches its maximum value. This format seems physically justifiable and produces profiles which match the data; although other shapes were tried (power law decline, Gaussian, etc.), the results were less satisfactory when compared with the observations. An additional modification is in the velocity structure: Not only can the radial velocity vary with distance from the star, but also the Doppler parameter, $q = (2kT/m + \xi^2)^{1/2}$, can change with position in the shell. (Here T is the temperature, m the atomic mass, and ξ the microturbulent velocity.) Both V and q vary linearly with distance: $V = V_1 + V_2r$, $q = q_1 + q_2r$.

The basic physical variables are the outer radius of the shell, R_{max} (the inner radius is taken as equal to the stellar radius); the density distribution within the shell, $\rho \propto r^{-n}$; the radial optical depth, T; the radial velocity at the star, V_*, and at the outer edge of the shell, V_r (or V_1 and V_2 related linearly); the Doppler parameter at the star, q_*, and at the outer edge, q_r, (or q_1 and q_2). The effect of the continuous stellar radiation is included as a star radiating with a gray, isotropic brightness specified in units of the Planck function while the line-forming region is in the extended, moving shell. It is assumed that in the shell itself there is no significant continuum emission or absorption.

a) *Line Breadths*

One of the significant features of the Fe II emission lines is their width. It is not clear where the actual zero level or background is above which the emission line is formed (see Fig. 2), but the full width at half-maximum (FWHM) measured from the zero level of the photospheric radiation is about 85 km s^{-1} for the 3228 Å line. A number of the physical parameters broaden the line, while others have no effect on the breadth. In the following study of these effects we show models with uniform velocity of infall of 10 km s^{-1} and a Doppler velocity of 10 km s^{-1}. Figure 3 shows that as the radial optical depth increases, as is well known, the line gets broader. The intensity also increases until the line becomes saturated after which the depth of the central absorption increases. Because of these latter two effects, we cannot match the line breadth by only increasing the optical depth. Figure 4 shows that the line widths increase with increasing fluid velocity, but that the degree of asymmetry is affected also. For uniform infall the red peak decreases relative to the blue peak. The effects of the Doppler parameter are shown in Figures 5*a*–5*c*. Figure 5*a* shows that as the Doppler velocity is increased the line width increases substantially, but the central absorption increases in width also. Figures 5*b* and 5*c* show the effects of a gradient in the Doppler velocity. If the Doppler parameter at the outer edge of the

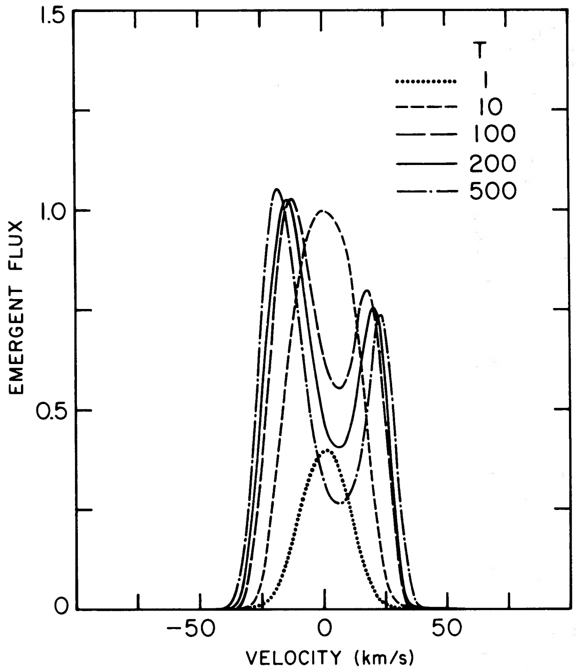

FIG. 3.—Calculated line profiles for various optical depths as indicated in the legend in the upper right. The basic parameters for Figs. 3–10 are uniform infall velocity of 10 km s^{-1}, microturbulence of 10 km s^{-1}, macroturbulence of 0 km s^{-1}, shell size of 2.5 R_*, optical depth of 200, density distribution following r^{-2}, a source function which peaks at 75% of the distance to R_{max}, and a gray isotropic core radiating with a brightness of 0.01, i.e., little continuum radiation. The solid curve in each figure corresponds to those basic parameters.

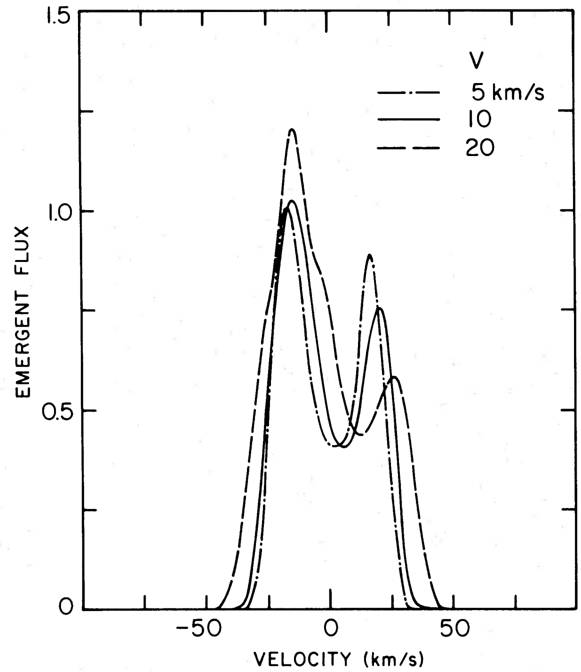

FIG. 4.—Calculated line profiles for various fluid velocities of uniform infall for T = 200 and the other parameters given for Fig. 3.

envelope is kept constant, but the value close to the star is increased from 5 to 10 to 15 to 30, as in Figure 5*b*, both the width and the line intensity are increased. Figure 5*c* shows the effect of changing the Doppler parameter at the outer edge while holding the value near the star constant at 10 km s^{-1}; both the emission and central absorption become broader.

Some of the variables have little influence on the line width. Figure 6 shows that increasing the shell size affects the ratio of the two peaks and the position of line center, but hardly increases the line width. The density used here falls off inversely with distance to the power n. As can be seen in Figure 7, whether that power is 1.5, 2, 3, or 4 has little effect on the whole profile including the breadth. We can adjust the place in the shell where the peak of the source function occurs, but this also has little effect on the width of the line as seen in Figure 8.

In order to account for the widths and the profile shapes of the strong lines, the inclusion of high velocities—Doppler and/or fluid—is inescapable. Since the temperature in the shell where the Fe II features are formed is not expected to be more than a few thousand degrees K, the Doppler velocity is due to nonthermal random motion. The effect of large-scale motions or macroturbulence, as seen in Figure 9, is to flatten the steep sides of the profile and to smear out the central absorption. The observed profile shapes rule out large-scale motions of more than about 10 km s^{-1}.

b) *Profile Shape and Position*

The physical characteristic that is primarily responsible for the position in wavelength of the Fe II emission in α Ori is the radial velocity in the shell. The position corresponding to the centroid of the emission is determined mainly by the velocity near the stellar surface, while the position of the central absorption is controlled by the velocity in the outer parts of the shell where the source function decreases, and the reversal is formed. Recall that both the Fe II emission and reversal are redshifted relative to the photosphere. Figures 10*a* and 10*b* show velocity gradients varying the value of the fluid velocity near the star and at the outer edge, respectively. A change in the velocity at the outer edge has a more dramatic effect on the profile shape (Fig. 10*a*) than a change near the stellar surface (Fig. 10*b*). The position of the red edge of the profile (and thus the line center) is more strongly affected by large velocities near the star than is that of the blue edge (Fig. 10*b*). The position of the reversal is influenced by the velocity at the outer edge (Fig. 10*a*). Large values of the velocity (~50 km s^{-1}) are needed before the line width is affected substantially.

As could be seen in Figure 3 the depth of the reversal is primarily due to the radial optical depth in the shell. The relative strengths of the two peaks are influenced by the shell size (Fig. 6), the fluid velocity (Figs. 4 and 10), and the turbulence (Fig. 5).

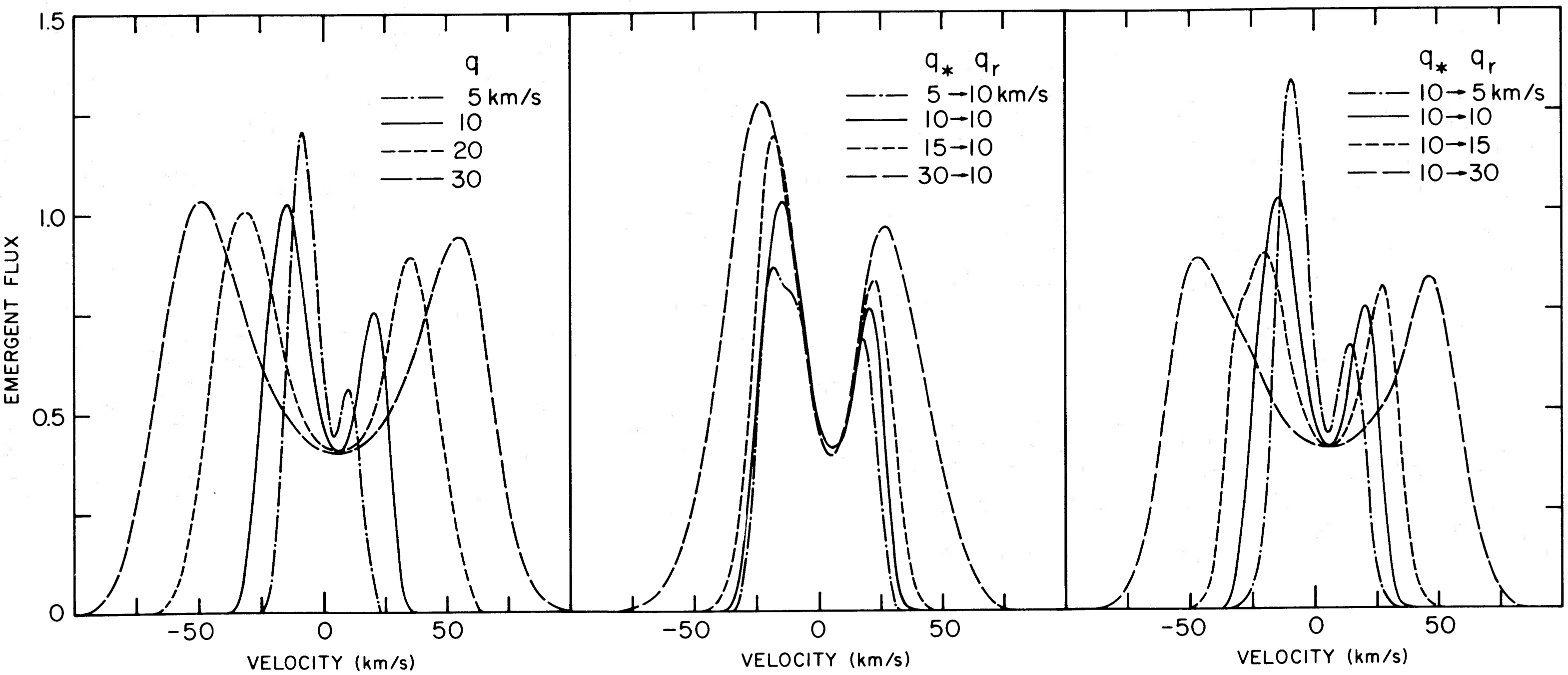

FIG. 5.—Calculated line profiles for a range of values of the microturbulence, q, and with other parameters given for Fig. 3. The left panel shows the results for uniform turbulence, while the center and right panels show the effect of gradients in the turbulent velocities where the turbulence at the other edge of the shell is 10 km s^{-1} and the inner edge is 10 km s^{-1}, respectively.

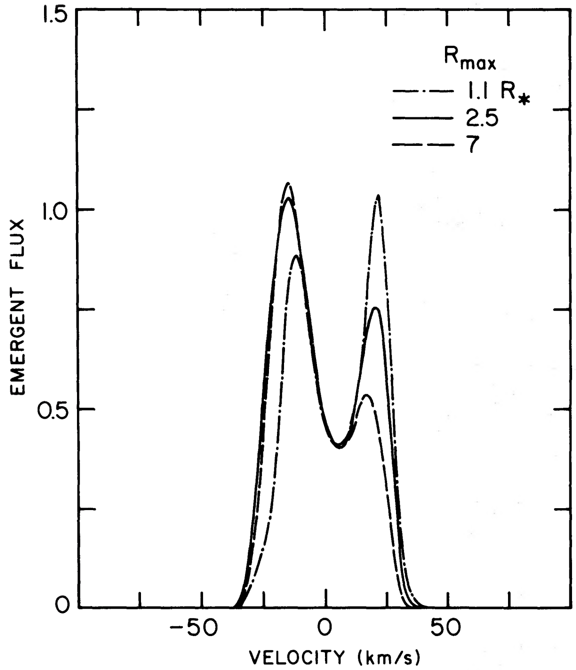

FIG. 6.—Calculated line profiles for the ratio, $R_{\max}/R_*$, and other parameters given for Fig. 3.

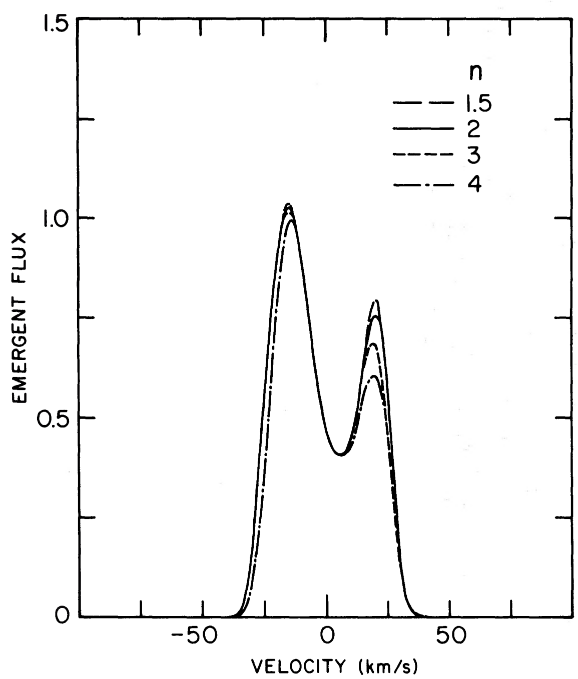

FIG. 7.—Calculated line profiles for different density distributions in the form $\rho \propto r^{-n}$ and for other parameters given in Fig. 3. Note that the density distribution has almost no influence on the profile shape.

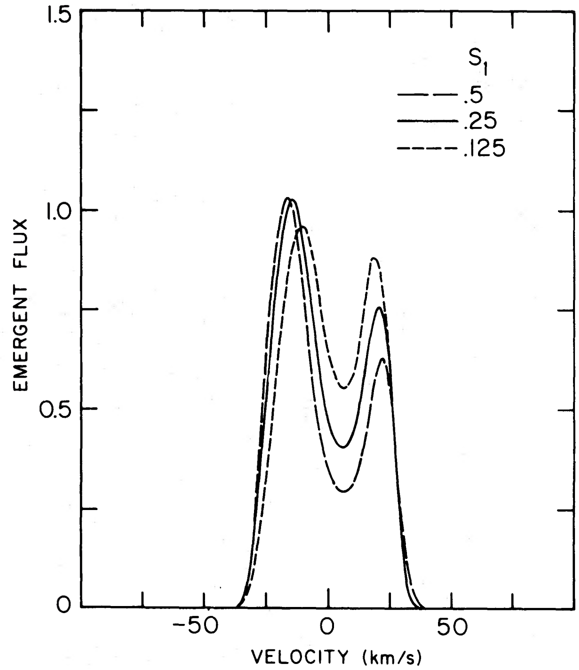

FIG. 8.—Calculated line profiles for values of S_1, the place in the shell where the source function reaches its maximum value, and for the other parameters given in Fig. 3. For S_1 = 0.25 the peak is 75% of the distance from R_* to $R_{\max}$, S_1 = 0.125 at 87.5% of that distance.

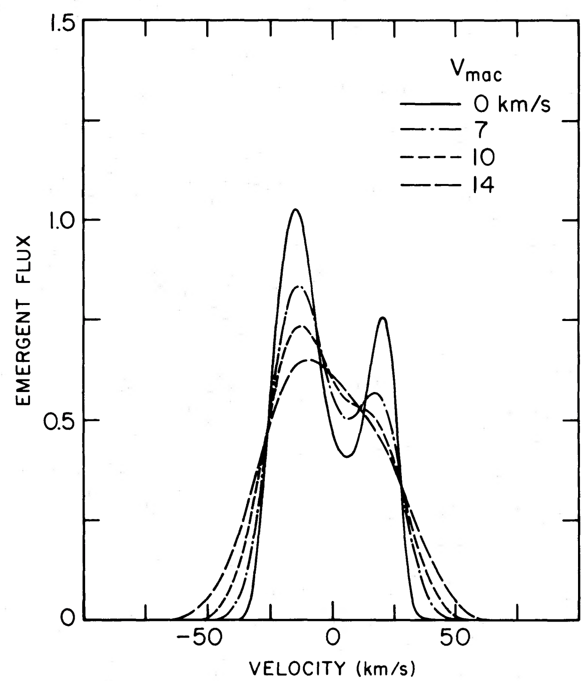

FIG. 9.—Calculated line profiles for a range of values for the macroturbulent velocity and other parameters given in Fig. 3.

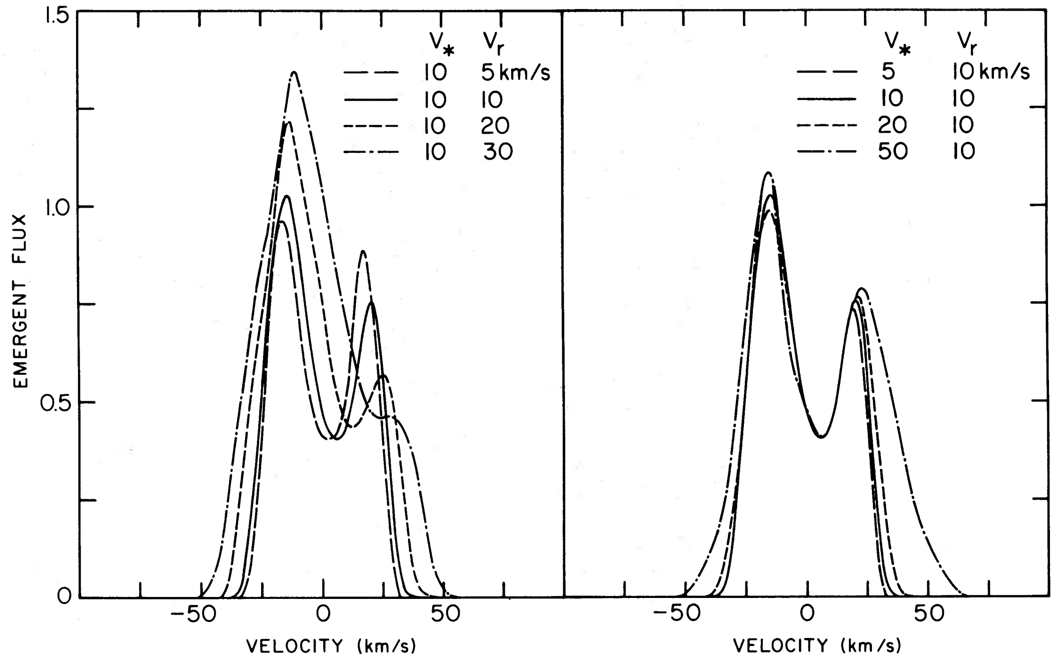

FIG. 10.—Calculated line profiles which show the effect of a gradient in the fluid velocity. The left panel shows a set where the inner shell velocity is 10 km s^{-1} of infall with a range of starting velocities at the outer edge. The right panel shows outer velocities of 10 km s^{-1} of infall toward a range of velocities at the stellar surface as indicated in the legend. Other parameters are as given in Fig. 3.

IV. OBSERVED AND THEORETICAL PROFILES IN α ORIONIS

The model was able to reproduce the observed profile of λ3228 and some of the weaker Fe II lines. The comparison between observed and computed profiles rests not only on the line shape and breadth but also on the position (radial velocity) of both the emission and the central reversal relative to the photospheric velocity. The *position* of the emission is basically determined by the fluid velocity close to the stellar surface, while the emission *width* results from the Doppler parameter and the fluid velocity. The position of the reversal and the width of the reversal are controlled by the fluid velocity and the Doppler velocity, respectively, near the outer edge, $R_{\max}$.

First, the profile of λ3228 was matched without taking the continuous photospheric radiation into account. The values for the shell size, turbulence, and optical depth thus derived are very similar to those found by Boesgaard and Magnan (1975) and provide a consistency check on the calculations. They commented that their calculated profiles (with uniform radial velocity) gave too small a redshift to match the observed value, but with a velocity gradient, and specifically a high infall rate near the surface, it was possible to match the observed radial velocity as discussed below. The Fe II emission is superposed on the stellar continuum and a more realistic calculation should include this effect. The observed peak intensity for λ3228 was set at 1.0 which places the local continuum at $\sim$0.3 as seen in Figure 2. The other Fe II lines were normalized to put the local continuum at 0.3. This value was used for the stellar-continuum contribution in the calculations. Introducing this contribution enhances the blue peak which can be countered by decreasing the extent of the shell. For these calculations also the source function peaks about 75% of the way from the stellar surface to the outer edge and the density decreases with r^{-2}.

Figure 11 shows the observed and computed profile for the λ3228 line including the stellar-continuum

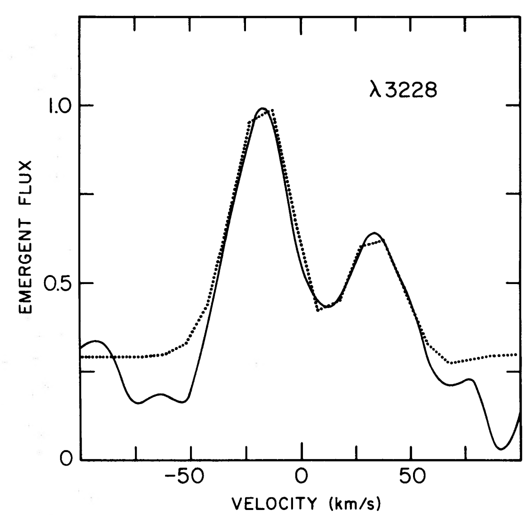

FIG. 11.—The observed profile for Fe II λ3228 (*solid line*) and the calculated profile (*dotted line*) which best matches it. The parameters for the fit are given in Table 3.

TABLE 3

SHELL PARAMETERS TO MATCH Fe II λ3228 LINE IN α ORIONIS

Parameters	Value	Range
Size of Fe II region	1.8 R_*	±0.1
Optical depth, T	500	±80
Fluid velocity, outer edge	18 km s^{-1}	±5
Fluid velocity near star	60 km s^{-1}	±5
Doppler velocity, outer edge	9 km s^{-1}	±2
Doppler velocity near star	9 km s^{-1}	±2
Macroturbulence	8 km s^{-1}	±2
Density distribution exponent	2	±1
S_1	0.25	±0.1
Core brightness	0.3	±0.05

contribution. The calculated parameters for this fit are given in Table 3 along with the maximum range of values for each parameter allowed by the data when the other parameters do not change. In order to match the observed redshifts of the emission and of the central reversal, it was necessary to introduce a gradient in the fluid velocity. The velocity increases inward from 18 km s^{-1} at 1.8 R_* to 60 km s^{-1} at the stellar surface. With the values quoted by Weymann (1978) for α Ori ($M/M_\odot = 14$ and $R/R_\odot = 633$), the free-fall velocity from 1.8 R_* to the surface is 61 km s^{-1}. The matter apparently is returning to the star accelerated by the gravitational field.

Section III*a* indicates that it is necessary to include a large Doppler parameter (as well as a high fluid velocity) in order to explain the line widths. The width of the Fe II line at λ3228 is about 85 km s^{-1}. The Doppler velocity found here is 9 km s^{-1} throughout the shell, i.e., no gradient was required in the nonthermal random motions. A similar value was found for the large-scale motions or macroturbulence: 8 km s^{-1}.

If the same basic model parameters could be found to yield profiles that fit the other emission lines by varying only the optical depth, the acceptability of the model would be improved. So in addition to the strong Fe II line at λ3228, two weak lines from the same multiplet were studied: λ3170 and λ3166. With a change in the optical depth only, both of these lines can be matched by profiles calculated with the same parameters as were derived for λ3228. Furthermore, the optical depths derived scale remarkably well with the relative *gf*-values given by Kurucz and Peytremann (1975); for λ3166, λ3170, and λ3228 the values of log *gf* are −2.95, −2.54, and −1.08, respectively, while log T values are 0.65, 0.85, and 2.70. For λ3166 a somewhat better fit is achieved when the velocity at the outer edge is reduced from 18 km s^{-1} to 12 km s^{-1}. Figure 12 shows those two observed lines and the calculated profiles which match. In addition computations were made for two other strong lines: λ3277 from multiplet 1 and λ3196 from multiplet 7. Again, line profiles calculated for smaller optical depths fit the observed profiles with the same parameters as were derived for λ3228. The actual fit is improved by a small adjustment in the fluid velocity at the outer edge; for λ3277 the best velocity is 11 km s^{-1}, and for λ3196 it is 15 km s^{-1} compared with 18 km s^{-1} for the stronger line λ3228. The observed and calculated profiles are shown for these two lines in Figure 13.

The linear relation between log *gf* and log T derived from the profile fit for the three lines in multiplet 6 provides an after-the-fact justification of the assumption that the same source function can be used for those lines. That the lines from the other multiplets (1) have similar excitation potentials to those in multiplet 6, and (2) fit the same linear relation reasonably well lends credence to having used the same form of the source function for them also.

V. DISCUSSION

The radial velocities of the Fe II and Ca II emission show that these features are redshifted relative to the

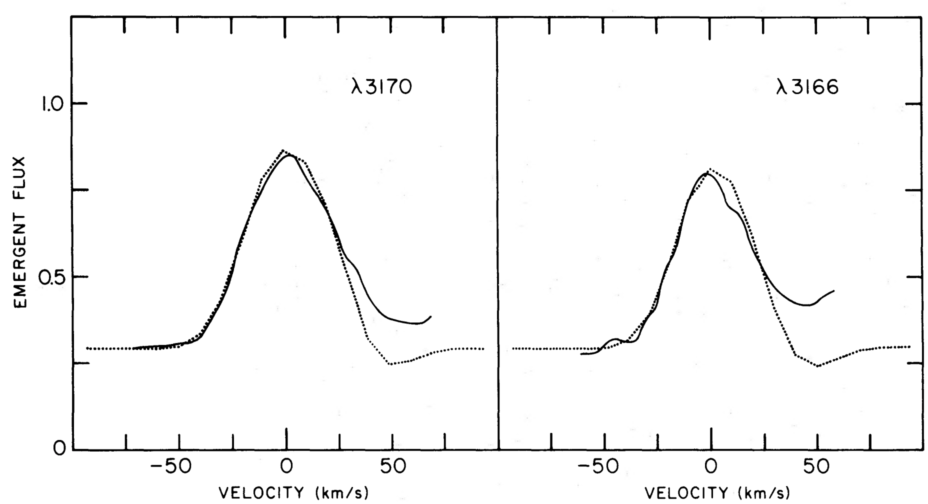

FIG. 12.—The observed (*solid line*) and calculated (*dotted line*) profiles for two weak lines: λ3170 and λ3166. The optical depths are T = 7 and 4.5, respectively. The other parameters of the fit are those listed in Table 3 except that an infall velocity of 12 km s^{-1} at the outer edge gives a better match for λ3166.

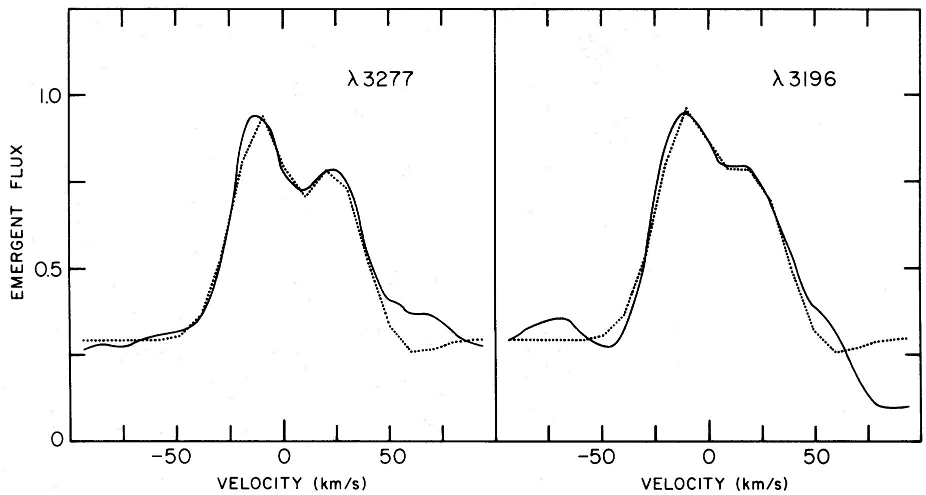

FIG. 13.—The observed (*solid line*) and calculated (*dotted line*) profiles for two other Fe II features: λ3277 and λ3196. The calculated optical depths are $T = 90$ for λ3277 and $T = 55$ for λ3196. The other parameters of the fit are given in Table 3 with the exception that the infall velocities at the outer edge of 11 km s^{-1} for λ3277 and of 15 km s^{-1} for λ3196 are shown here and give somewhat better fits.

photosphere by 5–6 km s^{-1}. Furthermore, Vaughan and Zirin (1968) indicate that the He I 10830 line may be present in α Ori with a strength of about 100 mÅ and a redshift of 10 km s^{-1}. However, recent Reticon spectra taken by O'Brien and Lambert (1979) show that *if* this feature is present, it has an equivalent width of ≤25 mÅ. The redshifts of Fe II, Ca II, and possibly He I imply infalling matter in the shell of α Ori. Wilson (1960) mentions several G supergiants which show redshifted K2 and/or K3 lines and conjectures that chromospheric material rises in a more ionized form and is seen falling back to the star. Measurements of the Fe II lines on six spectrograms of the M1 Ib star, α Sco, show that these emission lines are redshifted relative to the photosphere by an average of 7 km s^{-1} (Boesgaard, Chesley, and Kunasz 1977). The emission lines in α Ori at Fe II are up to 85 km s^{-1} in breadth, while the Ca II K2 feature is 186 km s^{-1} (Wilson and Bappu 1957). Bernat and Lambert (1976) measured the width at the base of the Mg II *k* emission line to be 410 km s^{-1}. These large line breadths presumably reflect the high non-thermal motions. Bernat and Lambert (1976) suggest that the Mn I and Fe I lines which cause the asymmetry in the Mg II *k* line are formed in a cool, turbulent layer above the chromosphere.

The detailed analysis of the Fe II line profiles leads us to a heuristic picture of high-velocity, infalling turbulent material in the inner shell region. The values for the fluid and Doppler velocities are the best determined of the parameters that affect the profile fit. The Fe II atoms producing the emission features are part of material falling back toward the star accelerating inward from 15–20 km s^{-1} to 60 km s^{-1}. At the surface of α Ori the velocity of sound is about 9 km s^{-1}, so material falling in at supersonic speeds of 60 km s^{-1} would produce a shock front. The observed Doppler motions and resultant broad emission features could result both from the turbulent eddies in the wake of the shocks and from the random motions in the gas caused by convective "overshoot" into the chromosphere from the few large convective cells hypothesized by Schwarzschild (1975). Since these cells would extend into the star about one-seventh of the stellar radius and cover only a few (2–5) pressure scale heights, convective overshoot upward into the envelope appears plausible. The deposition of this mechanical flux could also heat the chromosphere and produce emission lines where the stellar continuum is faint.

Although the material appears to be falling back toward the star at supersonic velocities, it is not necessary to invoke highly supersonic turbulence to account for the line widths. The microturbulence throughout the inner shell is about 9 km s^{-1}, while the large-scale motions are about 8 km s^{-1}. This fact is relevant to the mechanism of mass loss from the outer envelope; the absence of supersonic turbulence in the inner envelope may mean the absence of sufficient "turbulent support" to extend the material out to the dust-condensation point to produce mass loss as discussed by Weymann (1977).

It appears that a number of phenomena serve to move material upward into the extended atmosphere. Convective overshoot from the large photospheric convective cells of Schwarzschild is one, and this may be enhanced by whatever actual pulsation occurs in semiregular M supergiants. The fountaining atmosphere described by Spitzer (1939) with neutral atoms rising and ions falling is another. Wright (1970) has discussed late-type supergiants whose extended chromospheres eclipse early-type companions; gas condensations above the photosphere show velocities of many tens of kilometers per second and indicate supersonic, large-scale, non-Gaussian motions. A further means of extending the atmosphere is radiation pressure on molecules, especially CO, as proposed by Maciel (1976, 1977).

A complex picture emerges for the envelope of α Ori. The photosphere and chromosphere are extended. Upswelling material is driven by photospheric convection, giant fountaining or prominences, radiative pressure on molecules, etc. Some of this material returns to the surface of the star at high velocity. There are large turbulent motions in the medium of both large and small scale. Other material continues to move outward, possibly becoming supersonic at the base of the corona, and driving the mass loss through the hydrodynamic expansion of the hot corona as suggested by Mullan (1978). This material produces the violet-displaced absorption cores in the spectrum of α Ori which were studied in detail by Weymann (1962). Circumstellar dust has been observed at 10 μm in α Ori by Gehrz and Woolf (1971), among others, who propose that radiation pressure will act to drive the dust grains and the gas with it outward in the shell. [Fix and Alexander (1974) maintain that grains are an effect of mass loss, not a cause, because they cannot condense at chromospheric temperatures. However, as soon as grains *do* condense they will be accelerated outward by radiation pressure and this will contribute to mass loss.] The envelope extends outward to remarkable distances of several hundred stellar radii as observed in the K I line at λ7699 by Bernat *et al.* (1978).

I am indebted to Dr. P. Kunasz and Dr. D. G. Hummer for their generous help with instructions and information about their computer code and for many useful discussions about the physics involved. I am grateful to Duncan Chesley for his expert work in adapting the code for interactive use with the computer at the University of Hawaii and for several insights into the influence of the shell parameters on the line profiles. I wish to thank Graham Bromley for his contributions to the velocity measurements and Dr. Wendy Hagen for providing one of the spectrograms and most of the microphotometry. Part of this research was done while I was at the Nice Observatory and I appreciate the hospitality I received there. I have had many useful discussions with Drs. Ann Baglin, Hélène Frisch, John Jefferies, Christian Magnan, Martin Schwarzschild, and Ray Weymann. This research was supported by NSF grants AST 73-04840 and AST 76-81608.

REFERENCES

Bernat, A. P. 1977, *Ap. J.*, **213**, 756.
Bernat, A. P., Honeycutt, R. K., Kephart, J. E., Gow, C. E., Sandford, M. T., II, and Lambert, D. L. 1978, *Ap. J.*, **219**, 532.
Bernat, A. P., and Lambert, D. L. 1976, *Ap. J.*, **204**, 830.
Boesgaard, A. M. 1973, in *Stellar Chromospheres, IAU Colloquium* No. 19, ed. S. D. Jordan and E. G. Avrett (Washington, D.C.: NASA), p. 153.
Boesgaard, A. M., and Boesgaard, H. 1976, *Ap. J.*, **205**, 448.
Boesgaard, A. M., Chesley, D. M., and Kunasz, P. B. 1977, *Pub. A.S.P.*, **89**, 613.
Boesgaard, A. M., and Hagen, W. A. 1979, *Ap. J.*, **231**, 128.
Boesgaard, A. M., and Magnan, C. 1975, *Ap. J.*, **198**, 369.
Fix, J. D., and Alexander, D. R. 1974, *Ap. J.* (*Letters*), **188**, L98.
Gehrz, R. D., and Woolf, N. J. 1971, *Ap. J.*, **165**, 285.
Goldberg, L. 1976, *Mém. Soc. Roy. Sci. Liège*, 6 ser., **9**, 387.
Hagen, W. A. 1978, *Ap. J. Suppl.*, **38**, 1.
Herzberg, G. 1948, *Ap. J.*, **107**, 94.
Hummer, D. G., Kunasz, C. V., and Kunasz, P. B. 1973, *Computer Phys. Comm.*, **6**, 38.
Kunasz, P. B. 1974, Ph.D. thesis, Univ. of Colorado.
Kunasz, P. B., and Hummer, D. G. 1974, *M.N.R.A.S.*, **166**, 57.
Kurucz, R. L., and Peytremann, E. 1975, *Smithsonian Ap. Obs., Spec. Rept.*, No. 362.
Maciel, J. W. 1976, *Astr. Ap.*, **48**, 27.
———. 1977, *Astr. Ap.*, **57**, 273.
Mullan, D. J. 1978, *Ap. J.*, **226**, 151.
O'Brien, G., and Lambert, D. L. 1979, preprint, also 1978 *Bull. A.A.S.* **10**, 647.
Payne-Gasposchkin, C., and Gasposchkin, S. 1938, *Variable Stars*, Harvard Obs. Monograph No. 5 (Cambridge, MA: The Observatory).
Reimers, D. 1975, in *Problems in Stellar Atmospheres and Envelopes*, ed. B. Baschek, W. H. Kegel, and G. Traving (New York: Springer-Verlag), p. 227.
Sanner, F. 1976, *Ap. J. Suppl.*, **32**, 115.
Schwarzschild, M. 1975, *Ap. J.*, **195**, 137.
Spitzer, L. 1939, *Ap. J.*, **90**, 494.
Vaughan, A. H., and Zirin, H. 1968, *Ap. J.*, **152**, 123.
Weymann, R. J. 1962, *Ap. J.*, **136**, 844.
———. 1977, in *The Interaction of Variable Stars with Their Environment, IAU Colloquium* No. 42, ed. R. Kippenhahn, J. Rabe, and W. Strohmeier (Bamberg: Remeis-Sternwarte).
Wilson, O. C. 1960, *Ap. J.* **132**, 136.
Wilson, O. C., and Bappu, M. V. K. 1957, *Ap. J.*, **125**, 661.
Wright, K. O. 1970, *Vistas in Astronomy*, **12**, 147.

ANN MERCHANT BOESGAARD: Institute for Astronomy, University of Hawaii, 2680 Woodlawn Dr., Honolulu, HI 96822